Joint Special Interest Group meeting between euspen and ASPE
Advancing Precision in Additive Manufacturing
KU Leuven, Belgium, September 2023
www.euspen.eu

Adaptive masking for scaffold fabrication via high-resolution vat photopolymerization

Alberto Basso[1*], Javier Lopez Navas[1*], Marina Artemeva[1], Anna Danielak[1] and David Bue Pedersen[1]

[1] *Department of Civil and Mechanical Engineering, Technical University of Denmark*

albass@dtu.dk

Abstract
In the last decades, scaffold fabrication for tissue engineering has been a rising field. However, scaffolds are mainly produced via material extrusion (ME) and are limited to 2D or simple 3D structures that hardly imitate the in vivo conditions, thus hindering the efficiency of the structure to promote cellular proliferation and growth. Mask projection vat photopolymerization is a promising technology to improve scaffold fabrication. This method has the full capability to produce complex 3D structures on the microscale, offering the possibility to mimic the cell's natural environment and promote cell proliferation. Moreover, the versatility of vat photopolymerization (VPP) allows the manufacturing of scaffolds with a tuned surface topography to enhance cell adhesion. When fabricating microfeatures, one of the main challenges of VPP is overcuring. Due to the Gaussian nature of light, the irradiance will not be uniform throughout the mask, causing excessive crosslinking. This work shows a novel method that selectively switches off pixels of the projected slices to homogenize the light-intensity density across the exposed area, thus allowing the fabrication of smaller features with higher fidelity when compared with conventional VPP.

Vat Photopolymerization, Additive Manufacturing, Open Architecture, Adaptive Masking, Scaffold, Tissue Engineering

1. Introduction

The term tissue engineering was first used in the '90s when Roberts Langer and his team started investigating the use of a polymeric matrix (scaffold) as support to grow cells, since then, tissue engineering has been a fast-evolving discipline involving biology, material science, and engineering [1-4].

The fabrication of a scaffold with a 3D complex structure is of utmost importance, as it needs to be able to resemble organic anatomic shapes with both macro and micro feature sizes. Macroscopic features provide surgical fixation points between scaffolds and the human body while microscopic features serve to create a porous network that will promote cellular proliferation and growth [5].

Conventionally, scaffolds for tissue engineering were produced using different technologies, among others gas foaming [6-7], freezing drying [8-9], and sol-gel [10-11]; however, even though these techniques offer good ability in creating structures with small porosities, they failed in controlling pore structure and are inaccurate in fabricating customized parts [12].

Thanks to the inherited geometrical freedom and the ability to manufacture parts with high fidelity, additive manufacturing (AM) is a very promising discipline to produce scaffolds. The use of computer-aided-design (CAD) enables the design of scaffolds with desired porosities, providing parts with tailored pores in shape and size [13-14].

A widely used AM technique to produce scaffolds is material extrusion (ME). This technology is widely available, affordable, and simple to handle, nonetheless, ME does not offer sufficient accuracy during manufacturing [15-16]. The replication fidelity of ME is limited by nozzle size with a general dimension of 75 µm and by the poor ability to generate overhangs, a geometrical feature widely present in scaffolds [17-18].

An alternative method to manufacture scaffold parts is Vat Photopolymerization (VPP). VPP employs a structured ultraviolet (UV) light to crosslink a liquid photopolymer (also referred to as resin) into a tough structure. The parts are built in a layer-by-layer manner where the area exposed to irradiance is the cross-section of the produced part with a defined thickness [19-20]. The main advantages of VPP for scaffold fabrication are the tunability of the final viscoelastic properties and the process scalability as it offers a wide range of resolution-to-build envelope ratios [21]. VPP processes can fabricate features ranging from 1 µm to virtually any dimensions, depending on the light source system, with a building envelope between 10 mm^2 and 1 m^2 [22]. Furthermore, it offers high design flexibility and the possibility to fabricate complex structures in a single process, thus allowing for a high degree of customization and on-demand fabrication [23].

One of the challenges related to the VPP is the overcuring effect. Overcuring can be defined as excessive polymerization of the photosensitive resin due to inadequate chemical doping of the photopolymer or excessive light dose during UV exposure [24]. In light projection systems based on Digital Micromirror Devices (DMDs), a fraction of light reflected by each mirror overlaps the area corresponding to a neighboring mirror. Thus, in areas with high concentrations of powered pixels, the projected light reaches regions that lie beyond the targeted pixels, thus leading to overcuring. Consequently, the resolution of this fabrication technology is not limited solely by the pixel size (defined by the micromirror size), but rather by the overcuring ratio, which depends, among others, on the projected mask.

The present research takes advantage of such a phenomenon, homogenizing the light intensity distribution in the printing plane by selectively switching off pixels of the projected image. More specifically, this paper focuses on improving the part fidelity of a 90-degree grid scaffold fabricated via VPP.

Due to the tangled nature of the selected geometry, conventional process parameters adjustment has proven to be insufficient to successfully fabricate the holes in the center of the structure (henceforth referred to as pores). With the proposed adapted masks, not only do the pores become visible, but the fidelity of the fabricated grid is greatly improved. Moreover, the study shows how this alternative masking method allows for surface topography tuning, which could be used to boost cells' attachment to the scaffold.

2. Methodology

The scaffold design selected is a simple grid design with vertical and horizontal lines of 98 µm thickness, as seen in Figure 1, the scaffold has an overall dimension of 2.84x0.98x2.06 mm in length, height, and width respectively. The grid is constituted of four levels, starting with vertical lines on the top, the gap between lines measures 98 µm.

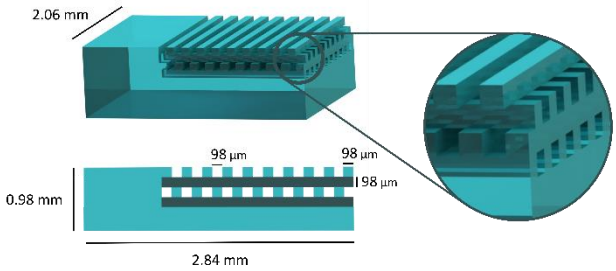

Figure 1. Renders of the designed scaffold. On the right, is the magnified detail of the scaffold grid.

To investigate the effect of the projected mask on the geometrical stability of the fabricated scaffold, five different projection patterns were utilized (including control). The light dosage excess is reduced by powering off entire rows of pixels. The highest energy dosage is provided by the control (100%), where all the pixels in the projected mask are set to an active state, and the minimum is case D (33%), in which two rows of pixels are switched off for every active row of pixel (see Figure 2). Case S is a special case where two patterns were projected alternatively for every layer, with an average energy dosage of 26% with respect to the control case. Figure 2 depicts the five masks used together with the reduction energy dosage with respect to control.

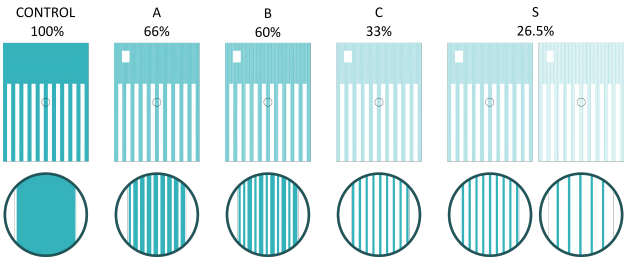

Figure 2. The five projected masks utilized to fabricate the scaffold. Only the vertical line mask is shown. The percentage indicates the energy dosage compared to the control mask.

Table 1 summarizes the most important process parameters used. Here, repositioning delay represents the waiting time between the moment in which the build plate is lowered to the defined position and the starting of light exposure. Longer repositioning delay allows the liquid photopolymer to reach a steady state, resulting in better replicating of the fabricated parts.

Table 1 Process parameters for scaffold fabrication.

Process parameters	Value
Layer Height	5 µm
Exposure time (Initial layers)	1.2 s
Irradiance (Initial layers)	0.10 W/cm^2
Exposure time	1.8 s
Irradiance	0.11 W/cm^2
Repositioning delay	2 s
Feed rate	2.5 mm/s

After fabrication, the samples were subjected to isopropanol rinse in an ultrasonic bath for 5 minutes at 30°C with a frequency of 80 kHz and then subjected to post-curing with 405 nm non-structured UV light for 5 minutes at 30°C

The photosensitive resin used for the fabrication of the scaffolds is BioScaffold3 from 3Dresyns. To achieve the best performance in a mask projection VPP system with 385 nm wavelength, the resin was tuned by adding 0.6 wt% of photoinitiator (commercially available as FT1 from 3Dresyn) and 0.8 wt% of UV-blocker (available as LB1 from 3Dresyns). The scaffolds were fabricated using the open architecture high-resolution VPP systems developed at the Technical University of Denmark. The setup is equipped with a Visitech LUXBEAM® LRS-WQ-HY light engine with a DMD chip DLP9000 DMD™ UV. The VPP open architecture has an interchangeable lens system, for this application a lens x0.5 was utilized, resulting in a reduction in pixel size to 3.77 µm. The open platform utilizes a high-precision linear stage from Physik Instrumente (PI L-511.03.5111), equipped with a DC motor and incremental linear encoder. Moreover, the setup is furnished with a rectangular shape self-peeling vat for a gentler detachment of the part from the membrane during the fabrication process [25].

The geometrical assessment of the samples was performed using the Olympus OLS 4000 LEXT laser confocal microscope and the data were processed using the image analysis software MountainMap®.

3. Results and discussion

In this study, the performance of four optimized masks (A, B, C, and S) with a control sample was compared in terms of reduction of overcuring and standard deviation. Figure 3 shows how overcuring occurring in the control sample is more perceptible toward the center of the scaffold, where the

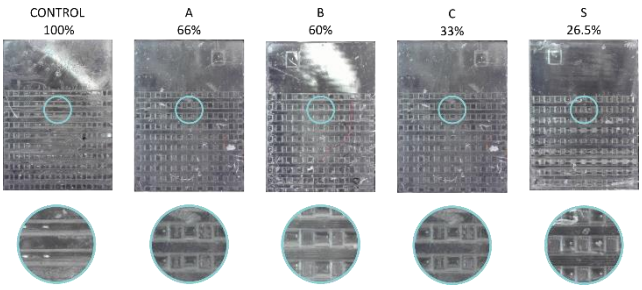

Figure 3. Five samples, one for each projected mask. The percentage indicates the energy dosage compared to the control mask.

fabricated lines tend to get thicker, and the pores are no longer visible.

In contrast to control, all the other masking strategies show a more uniform line width across the scaffold as well as a visible inner grid.

Figure 4 illustrates the average values of line width and pore depth for the manufactured scaffold grid, with two bar charts displaying a comparison between the dimensions of the four

optimized masks and the dimensions of the control samples. Overcuring can be observed as the standard deviation for the line width is up to 7.6 times higher in the control with respect to a modified mask. Moreover, Figure 4 shows that all the proposed masks lead to line widths closer to their nominal value compared to the control mask. Results close to the nominal value were achieved for samples A and B with an average energy dosage of 66% and 60% with respect to the control sample. Samples C and S showed line width below the nominal value, indicating undercuring and thus the need for further process parameter optimization.

The high degree of overcuring for the control samples resulted in pore depths close to zero, as most pores of the control scaffolds were completely clogged. In this regard, the study demonstrates an effective way to increase the pore depth for the fabricated scaffolds. However, only samples from case C reached a pore depth close to the nominal dimension, while the other samples tend to fall below the nominal value.

High standard deviations were detected, particularly for cases A, B, and S; thus, indicating the existence of other factors affecting the pore depth. A likely cause for the low pore depth can be explained by considering the post-processing strategy. After fabrication, the pores of the scaffolds are filled with uncured resin which should be removed by cleaning with isopropyl alcohol. Cleaning very small crevices, like the pore in the scaffold, can be a challenging task. An incomplete cleaning results in pores partially filled with uncured resin that is later cured in the post-curing process, explaining the low pore depth observed in the fabricated parts. On the other hand, on average, the samples for case C displayed lower line width. A reduction in line width results in wider pores. An increase in the width of the pores would ease the cleaning process, justifying the higher pore depth exhibited by these samples.

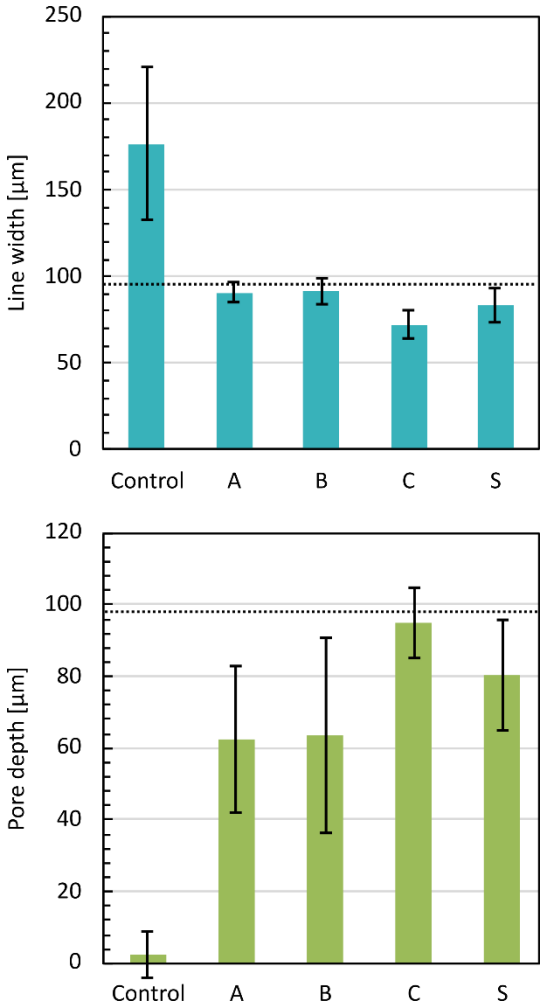

Figure 4. Average line width (above) and average pore depth (below) of the fabricated scaffolds. Dashed lines indicate the nominal value equal to 98 µm.

Besides the geometrical compliance, the surface topography was also investigated. Researchers showed that cell proliferation can be improved by modifying the surface topography [26]. This study investigated the possibility to use mask adaptation to tailor the surface finishing of the fabricated scaffolds.

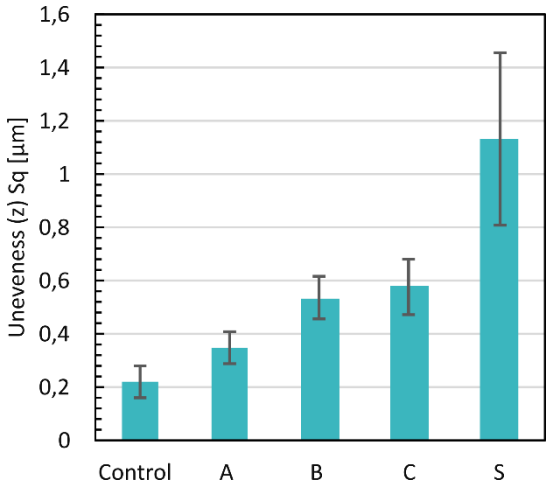

Figure 5. Height unevenness of the primary surface for the fabricated samples.

Figure 5 depicts the height unevenness of the surfaces for the control samples and the scaffolds fabricated using the four different projected patterns. Overall, all adapted masks show a more uneven surface compared to the control sample. This shows that the overcuring effect is not strong enough to fully cure the neighboring unprojected areas from the adapted masks. Consequently, different patterns lead to different levels of surface unevenness.

In this regard, this method is proved to be a powerful tool to manipulate the surface topography of the fabricated part in a controlled manner, thus being able to fabricate parts with tuned surface unevenness for specific cell types.

4. Conclusion

The study showed that reducing light dosage through mask adaptation has a beneficial effect in mitigating overcuring. The line widths of the adapted mask samples are closer to the nominal value compared to the control masks, as well as the pores are visible through the whole geometry. However, further process optimization is required by evaluating different masking strategies, modifying the process parameters, and exploring alternative, moderate approaches to minimize the adverse effects of post-processing, such as using harsh solvents.

Furthermore, the results revealed that the surface topography can be tuned depending on the masks used. While low values are generally desired for an excellent surface finish, there are other applications, namely tissue engineering, where specific surface unevenness intervals will boost the performance of the fabricated part.

Overall, the optimization of the projected mask dimensions in scaffold manufacturing for tissue generation showed promising results in reducing overcuring, improving dimensional accuracy, and offering control over surface topography. These findings provide valuable insights for further advancements in the field

of scaffold fabrication, paving the way for enhanced tissue engineering.

5. Future work

One research direction should be focused on refining the process parameters to achieve a closer alignment with the nominal values for line width and pore depth of the optimized scaffolds. Additionally, alternative cleaning techniques and strategies to prevent layer detachment should be investigated to mitigate the potential deviations observed in the optimized samples. Moreover, it will also be necessary to further characterize how the different masks affect the surface topography in depth (e.g., roughness and waviness). By understanding how the different masks influence the different surface texture parameters, it will be possible to tailor the surface finish according to specific application requirements.

Acknowledgments

Grundfos Foundation for the Open Additive Manufacturing Initiative grant.

Remarks

* The authors contributed equally to this work.

References

[1] Scott J. Hollister, 2009 *Advanced Materials*. **21** 32-33 https://doi.org/10.1002/adma.200802977

[2] Mark E. Furth, Anthony Atala,2014 Tissue Engineering: Future Perspectives. *Principles of Tissue Engineering* . 83-123 https://doi.org/10.1016/B978-0-12-398358-9.00006-9

[3] Randall E. McClelland, Robert Dennis, Lola M. Reid, Jan P. Stegemann, Bernard Palsson, Jeffrey M. Macdonald, 2012 Tissue Engineering. *Introduction to Biomedical Engineering.* 273-357 https://doi.org/10.1016/B978-0-12-374979-6.00006-X

[4] François Berthiaume, Martin L. Yarmush, 2003, Tissue Engineering *Encyclopedia of Physical Science and Technology. 817-842.* https://doi.org/10.1016/B0-12-227410-5/00783-3

[5] Scott J. Hollister, 2005 Porous scaffold design for tissue engineering. *Nat Mater.* **4** 518-524 https://doi.org/10.1038/nmat1421

[6] Moghadam M Z, Hassanajili S, Esmaeilzadeh F, et al. 2017, Formation of porous HPCL/LPCL/HA scaffolds with supercritical CO_2 gas foaming method. *J Mech Behav Biomed Mater.* **69**:115. https://doi.org/10.1016/j.jmbbm.2016.12.014

[7] Costantini M, Colosi C, Mozetic P, et al. 2016, Correlation between porous texture and cell seeding efficiency of gas foaming and microfluidic foaming scaffolds. *Mater Sci Eng C Mater Biol Appl.* **62**:668–677 https://doi.org/10.1016/j.msec.2016.02.010

[8] Abdkhorsand S, Sabersamandari S. 2017, Development of nanocomposite scaffolds based on TiO_2 doped in grafted chitosan/hydroxyapatite by freeze drying method and evaluation of biocompatibility. *Int J Biol Macromol.* **101**:51–58. https://doi.org/10.1016/j.ijbiomac.2017.03.067

[9] Fereshteh Z, Fathi M, Bagri A, et al. 2016, Preparation and characterization of aligned porous PCL/zein scaffolds as drug delivery systems via improved unidirectional freeze–drying method. *Mater Sci Eng C Mater Biol Appl.* **68**:613–622 https://doi.org/10.1016/j.msec.2016.06.009

[10] Theodorou G S, Eleana K, Anna T, et al. 2016, Sol–Gel derived Mg–based ceramic scaffolds doped with zinc or copper ions:Preliminary results on their synthesis, characterization, and biocompatibility. *Int J Biomater.* **2016** :3858301 https://doi.org/10.1155/2016/3858301

[11] Ros–Tárraga P, Murciano A, Mazón P, et al. 2017, New 3D stratified Si–Ca–P porous scaffolds obtained by sol–gel and polymer replica method:Microstructural, mineralogical and chemical characterization. *Ceram Int.* **43**(8):6548–6553 https://doi.org/10.1016/j.ceramint.2017.02.081

[12] Yang Y, Wang G, Liang H, Gao C, Peng S, Shen L, Shuai C, 2018, Additive manufacturing of bone scaffolds. *Int J Bioprint*. **148** https://doi.org/10.18063/IJB.v5i1.148

[13] Chen Hao, Han Qing, Wang Chenyu, Liu Yang, Chen Bingpeng, Wang Jincheng, 2020, Porous Scaffold Design for Additive Manufacturing in Orthopedics: A Review. *Frontiers in Bioengineering and Biotechnology*. **8** https://doi.org/10.3389/fbioe.2020.00609

[14] Bandyopadhyay, A.; Vahabzadeh, S.; Shivaram, A.; Bose, S. 2015, Three-dimensional printing of biomaterials and soft materials. *MRS Bull.* ***40***, 1162–1169 https://doi.org/10.1557/mrs.2015.274

[15] Vaezi Mohammad, Zhong, Gaoyan, Kalami Hamed, Yang, Shoufeng, 2018, Extrusion-based 3D printing technologies for 3D scaffold engineering. *Functional 3D Tissue Engineering Scaffolds* https://doi.org/10.1016/B978-0-08-100979-6.00010-0

[16] Xin Wang, Man Jiang, Zuowan Zhou, Jihua Gou, David Hui, 2017, 3D printing of polymer matrix composites: A review and prospective. *Composites Part B: Engineering.* **110** 442-458 https://doi.org/10.1016/j.compositesb.2016.11.034

[17] Christopher M. O'Brien, Benjamin Holmes, Scott Faucett, and Lijie Grace Zhang, 2015, Three-Dimensional Printing of Nanomaterial Scaffolds for Complex Tissue Regeneration. *Tissue Engineering Part B: Reviews.* **21** 103-114 https://doi.org/10.1089/ten.teb.2014.0168

[18] Fu, Q., Saiz, E., & Tomsia, A. P., 2011, Direct ink writing of highly porous and strong glass scaffolds for load-bearing bone defects repair and regeneration. *Acta Biomaterialia.* **7** 3547-3554 https://doi.org/10.1016/j.actbio.2011.06.030

[19] Gibson, I., Rosen, D., & Stucker, B., 2015, Vat Photopolymerization Processes. In Additive Manufacturing Technologies. *Springer New York.* 63-106 https://doi.org/10.1007/978-1-4939-2113-3_4

[20] Oscar Santoliquido, Paolo Colombo and Alberto Ortona, 2019, Additive Manufacturing of ceramic components by Digital Light Processing: A comparison between the “bottom-up” and the “top-down” approaches. *Journal of the European Ceramic Society.* **39** 2140-2148 https://doi.org/10.1016/j.jeurceramsoc.2019.01.044

[21] Ali Bagheri and Jianyong Jin, 2019, Photopolymerization in 3D Printing. *ACS Applied Polymer Materials.* **1.4** 593-611 https://doi.org/10.1021/acsapm.8b00165

[22] Qi Ge et al., 2020, Projection micro stereolithography based 3D printing and its applications. *International Journal of Extreme Manufacturing.* **2.2** https://doi.org/10.1088/2631-7990/ab8d9a

[23] Mohsen Attaran, 2017, The rise of 3-D printing: The advantages of additive manufacturing over traditional manufacturing. *Business Horizons.* **60.5** 677-688 https://doi.org/10.1016/j.bushor.2017.05.011

[24] Paul O’Neill, Nigel Kent, 2017, Mitigation and control of the overcuring effect in mask projection micro-stereolithography. *AIP Conference Proceedings.* **1896** https://doi.org/10.1063/1.5008249

[25] Ribo, M. M., Danielak, A. H., Islam, A., & Pedersen, D. B. (2019). Optimization of a self-peeling vat for precision vat photopolymerization setups. In euspen's 19th International Conference & Exhibition (pp. 234-237). The European Society for Precision Engineering and Nanotechnology.

[26] Huang, H. H., Ho, C. T., Lee, T. H., Lee, T. L., Liao, K. K., & Chen, F. L. (2004). Effect of surface roughness of ground titanium on initial cell adhesion. *Biomolecular engineering*, **21**(3-5), 93-97.